Communication

Simple RF design for human functional and morphological cardiac imaging at 7 tesla

M.J. Versluis [a], N. Tsekos [b], N.B. Smith [a], A.G. Webb [a,*]

[a] C.J. Gorter Center for High Field MRI, Department of Radiology, Leiden University Medical Center, Leiden, The Netherlands
[b] Computer Science Department, University of Houston, Houston, USA

ARTICLE INFO

ABSTRACT

Morphological and functional cardiac MRI can potentially benefit greatly from the recent advent of commercial high-field (7 tesla and above) MRI systems. However, conventional hardware configurations at lower field using a body-coil for homogeneous transmission are not available at these field strengths. Sophisticated multiple-transmit-channel systems have been shown to be able to image the human heart at 7 tesla but such systems are currently not widely available. In this paper, we empirically optimize the design of a simple quadrature coil for cardiac imaging at 7 tesla. The size, geometry, and position have been chosen to produce a B_1 field with no tissue-induced signal voids within the heart. Standard navigator echoes for gating were adapted for operation at the heart/lung interface, directly along the head–foot direction. Using this setup, conventional and high-resolution cine functional imaging have been successfully performed, as has morphological imaging of the right coronary artery.

© 2009 Elsevier Inc. All rights reserved.

1. Introduction

The majority of high-field MRI studies have focused on the brain, with developments such as transmit arrays [1], contrast optimization [2] and RF pulse design for increased B_1 homogeneity [3] forming a few of the areas of active technical research. Musculoskeletal imaging at 7 tesla has also seen a recent surge in activity [4–6]. Abdominal imaging is acknowledged to be the most challenging area for high-field MRI due to the large dimensions of the torso. The fact that these dimensions are now significantly greater than the wavelength of the electromagnetic (EM) radiation in tissue result in sample induced inhomogeneities in the transmitted and received B_1 fields. The complex wave behavior can also cause electric field "hot-spots", resulting in raised local heating. Similar effects in the field of electromagnetic hyperthermia have been known for many decades, as has the solution of using transmit arrays with different magnitudes and phases applied to each element of the array [7,8]. In MRI terms, this process has been termed "B_1-shimming" [9], in which the spatial distributions of the magnetic component of the EM field is the major focus of the optimization strategy.

Only recently has it been shown that whole-body imaging is feasible at 7 tesla and above [10]. The authors showed results from both an actively detunable TEM resonator combined with multichannel stripline detector, and a full transmit array [10]. Specific

results have also been shown for the heart using this type of RF hardware [11]. This approach can be considered as the optimum engineering solution, but does require extensive hardware design and construction, and a very high level of technical skill to implement successfully. The purpose of our current study was to determine whether a much more simple approach could be used to acquire both morphological and functional cardiac images of clinical utility at 7 tesla.

In terms of cardiac imaging, the pros and cons of moving from lower to higher magnetic fields have been discussed previously in [12] and references therein, comparing 1.5 and 3 tesla: such considerations are also pertinent when considering cardiac imaging at 7 tesla. Briefly, the advantages of higher fields include improved tagging due to the prolonged T_1 time of the myocardium, improved perfusion imaging both due to the increased signal-to-noise (S/N) and the longer myocardial T_1 values, and a higher velocity-to-noise ratio in blood velocity measurements. Specific challenges outlined in [12] included implementation of high efficiency balanced SSFP sequences without off-resonance banding artifacts, the detrimental effects of B_1 and B_0 inhomogeneity on inversion-recovery prepared sequences in particular, and the high potential specific absorption ratio (SAR). Although not mentioned, localized MR spectroscopy is also an area that should profit considerably from the higher field. Based upon these observations, the potential of cardiac imaging at 7 tesla appears very high.

In this paper we show that a simple RF coil configuration can be used to acquire high quality cardiac images at 7 tesla. The geometry of a quadrature transmit/receive surface coil was optimized to achieve coverage across the entire heart, enabling acquisition of functional cine images in both four-chamber and two-chamber

cross-sections, as well as morphological images of the right coronary artery (RCA).

2. Materials and methods

All experiments were performed using a Philips Achieva 7 tesla whole body system. The system has a single proton RF transmit channel, with two quadrature ports available on the RF interface box, through which custom-built coils can be connected via simple type-N connectors. The maximum power from the RF amplifier is 4 kW, with approximately a 50% loss through cabling between the amplifier and coil interface and transmit/receive switches: the maximum available power for each quadrature channel is therefore ~1 kW. All experiments were approved by the Commissie Medische Ethiek at the Leiden University Medical Center.

2.1. RF coil geometry

In addition to improving the S/N, quadrature coils help to alleviate the B_1 inhomogeneities encountered at high field [13]. In this study, the different quadrature coil configurations tested included overlapped circular and rectangular loops, rectangular loops with central common capacitors [14], and loop/butterfly pairs [15]: this list is certainly not exhaustive, but represents the most commonly used configurations. For a given size, the performance of each coil was assessed in terms of B_1 homogeneity and S/N. Any coil arrangement that produced a significant dark "banding" within the image was discarded, irrespective of the S/N. Empirically, we observed that the optimum arrangement was the loop/butterfly pair. As described by Kumar and Bottomley [16], for circular loops the geometry that produces the maximum intrinsic S/N (excluding system and conductive losses in the detector) at a depth d is given at low frequencies by $r_0 = d/\sqrt{5}$ and $r_8 = 0.6d$, where r_0 is the radius of the single loop, and r_8 that of each half of the butterfly coil. The distance to the center of the heart from the surface of the chest in a typical volunteer was

approximately 10 cm: the single loop was placed 2 cm above the chest, and the butterfly coil 1 cm above the chest, in accordance with the "liftoff" phenomenon described by Suits et al. [17]. These numbers give values of 10.8 cm for the diameter of the single loop and 13.2 cm for the diameter of each loop of the butterfly coil. Upon testing, it was found that these dimensions did not give sufficient penetration for the posterior part of the heart to be seen with sufficient S/N, and so the dimensions were increased successively until the heart could be fully visualized. The values determined empirically were 15 cm diameter for the single loop and 18 cm diameter for each loop of the butterfly coil. The RF coils were segmented into conductor lengths of 6 cm, corresponding to $\sim\lambda/16$ at 298 MHz, using 3.9 pF non-magnetic capacitors (ATC, Series B, Huntington Station, NY). Three variable capacitors (1-40 pF, Johansson, Camarillo, CA) were used for fine tuning and impedance matching in a balanced configuration. A lattice balun was used to improve the balance of the coil. Finally, a 1 cm diameter gap, filled with foam, was used between the coil and patient to avoid very heavy sample losses [17]. Fig. 1a–c show schematics and a photograph of the coil geometry and placement on the subject. Network analyzer measurements were performed on the patient outside the magnet and, after fine tuning, the S_{11} and S_{22} parameters were both less than −20 dB, with the S_{21} between −18 and −24 dB for all patients studied. The unloaded and loaded Q values were measured to be 186 and 18, respectively. There is a negligible frequency shift when the coil is placed on the patient since the 1 cm spacer reduces the interaction of the strong electric fields around each capacitor with the body.

2.2. Vector electrocardiogram (vEKG)

A four-channel commercial vector ECG (VECG) module was used to trigger from the R-wave. Despite the well-known magneto-hydraulic effect, EKG's were obtained in the vast majority of cases without the need for electrode repositioning, as has also been reported by Snyder et al. [11].
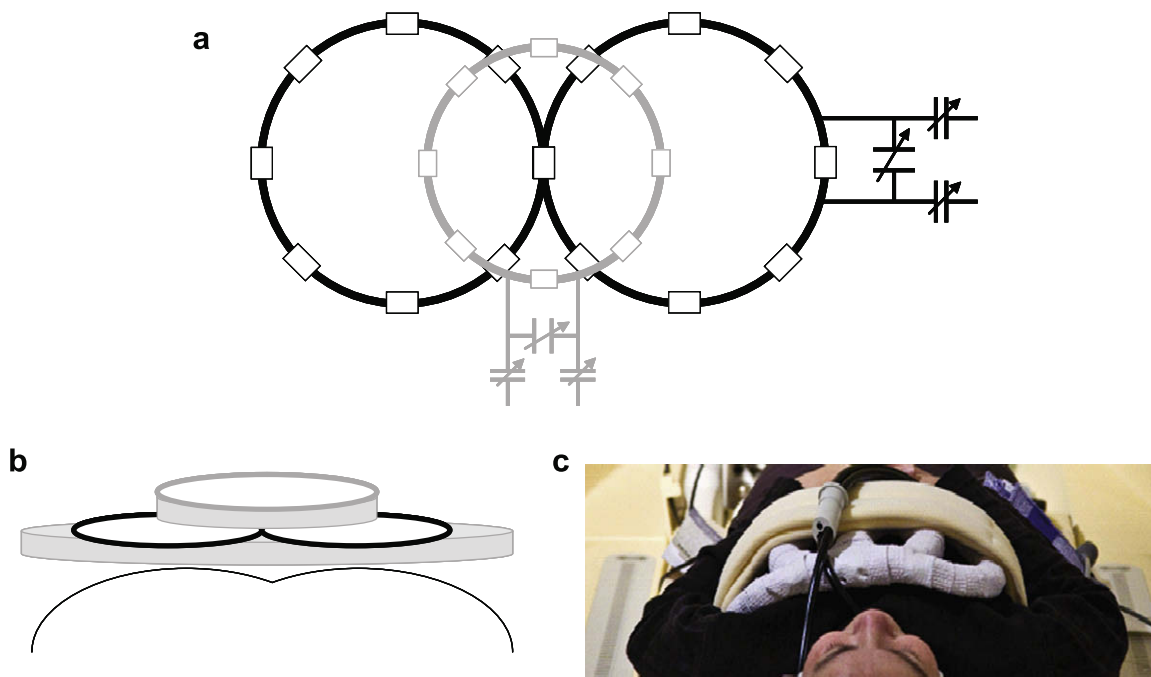
Fig. 1. (a) Schematic of the single loop (gray lines)/butterfly coil (black lines) configuration. Capacitors are denoted by the small boxes. The impedance matching networks are shown for each coil. (b) Physical placement of the coils on the subject's chest. The shaded regions represent open-core foam of thickness 1 cm. (c) Photograph of the coil assembly placed on top of the volunteer, and interfaced to the quadrature transmit/receive box of the Philips 7 tesla.

2.3. Navigator gating

Navigator echo gating was used for imaging the right coronary artery (RCA) using a "pencil-beam" navigator. Conventional navigator gating has the pencil beam centered on the right hemidiaphragm, at the lung/liver interface in a head/foot direction. Since coverage was limited in the head/foot direction using the surface coil setup, we adapted the pencil beam to be situated at the heart/lung interface, but maintaining the head/foot direction of the navigator. This approach was based on previous experience of coronary artery imaging at 7 tesla [18], and proved to be highly reproducible despite the relatively small surface area perpendicular to the navigator beam, as compared to the conventional configuration.

2.4. Cine imaging

Cine images were acquired using a segmented gradient echo sequence with RF spoiling and crusher gradients to eliminate transverse magnetization. A TURBOFLASH gradient echo sequence was used for prescribing the short-axis views planes for cine imaging. Multislice cine scans were acquired in multiple breath-holds (acquiring one or two slices per breath-hold).with the following parameters: TR/TE = 4 ms/2.4 ms, tip angle = 20°, voxel size = $1.3 \times 1.4 \times 8$ mm^3, 12–14 slices. VECG triggering was used retrospectively to reconstruct 33 heart phases. High-resolution cine images were acquired for a single slice in a breath-hold of ∼20 s with the following parameters: TR/TE = 5.4/3.4 ms, tip angle = 20°, voxel size = $0.65 \times 0.7 \times 8$ mm^3.

2.5. Coronary artery imaging

The procedure for acquisition of the coronary artery geometry is described in detail elsewhere [18]. To summarize, the basic steps are to acquire scout scans for the visual identification of the time period (Td) of minimal coronary motion. The scan plane is then localized parallel to the RCA. Free-breathing 3D coronary MRA (segmented k-space gradient-echo imaging, TR = 4 ms, TE = 1.5 ms, RF excitation angle = 15°, field-of-view = 320×291 mm^2, scan matrix = 392×373, 15 slices, slice thickness = 2 mm, acquisition window ∼100 ms, scan time ∼5 min) was performed using prospective navigator gating with the 2D selective navigator localized at the heart–lung interface. Image data were collected in mid-diastole at the predetermined time Td. An adiabatic spectrally selective inversion recovery module with inversion time (TI) = 305 ms was used for fat suppression to enhance the endogenous contrast between the coronary blood-pool and epicardial fat.

2.6. Estimation of B_1^+ for SAR calculations

The B_1^+ field was estimated using an interleaved dual repetition FLASH sequence which allows a direct calculation of the tip angle distribution [19]. The following parameters were used: TR$_1$/TR$_2$/TE = 15/75/1.0 ms, tip angle = 40°, voxel size = $2.3 \times 4.6 \times 15$ mm^3, 15 signal averages, total scan duration was 3 min. Images were acquired in the transverse plane for measurements at the chest surface and also at the center of the heart. Fifteen signal averages were acquired to reduce the effects of heart motion on the estimated B_1^+ map. It should be noted that the results obtained are only estimations, and are not absolutely quantitative due to the fact that, for practical purposes of scanning time, the maps were acquired in 2D rather than 3D scans [20]. Because of the thick slice and the number of averages the effect that respiratory and cardiac motion have on the steady state magnetization is expected to be minimal.

3. Results

3.1. Coil performance

Fig. 2 shows images acquired with three different RF coil configurations using a low flip angle, low-resolution TURBOFLASH sequence to assess the B_1 profile of each configuration. Fig. 2a uses a single loop coil, and displays minor non-uniformity in the image, as predicted by a number of previous studies. Fig. 2b shows the results of using the loop/butterfly combination driven in quadrature, with not only the expected increase in penetration depth, but also an improvement in the B_1 uniformity. The improvement in B_1 may also be indirectly appreciated considering the increased CNR between the septal wall and the two ventricles, the improved B_1 results correspond to a higher effective flip angle. It should be noted that the symmetric sensitivity profile of the quadrature coil arises from the combination of two asymmetric fields, the B_1^+ transmit field and the B_1^- receive field, as described previously by Wang et al. [21]. Fig. 2c is illustrative, in the sense that the two coils are driven in an anti-quadrature configuration, and gives a good indication of areas in which the B_1 fields of the two coils are orthogonal.

3.2. Cine-scans

Individual frames of a cine sequence at a "conventional" spatial resolution of $1.3 \times 1.4 \times 8$ mm are shown in Figs. 3 and 4 for the short-axis and four-chamber configurations, respectively. There is excellent blood/myocardium contrast and no areas of B_1 inhomogeneity beyond those which are associated with the intrinsic drop-off of B_1 amplitude from a surface coil. The S/N of the myocardium was measured to be between 10 and 25:1 depending on the particular area of the myocardium, the S/N of the left ventricle was between 20 and 40:1.

In order to take advantage of the high sensitivity of the 7 tesla, a high-resolution cine scan was run on one volunteer. Images with a spatial resolution of $0.65 \times 0.7 \times 8$ mm are shown in Fig. 5. Although the S/N is obviously reduced compared to the images in Figs. 3 and 4, there is much finer definition of the cardiac muscles.

3.3. Coronary artery imaging

Fig. 6 shows successive slices in which the right coronary artery can be easily visualized, together with an expanded view for clarity. There is good contrast between the artery and the surrounding tissue, allowing clear delineation of the artery walls.

3.4. SAR estimation

In all high field human studies, an important issue is the SAR, both in terms of local and average values. Despite some initial promising studies using direct MRI temperature measurements in vivo, it remains extremely challenging to measure SAR directly, and so most estimations are based on computer simulations. Since blood perfusion is not included in the majority of simulations, one must also recognize that such simulations represent "worst-case" scenarios in terms of causing actual tissue heating.

We have based our SAR estimations on previous work by Collins and Smith [22], who specifically modeled the SAR for a surface coil adjacent to an anatomically-correct human body model. The regions of highest SAR were found to be at the right medial portion of the pectoral muscle near the superior end of the sternum: the SAR in the heart itself is extremely low. The authors provide appropriate scaling factors for setups different than the particular one
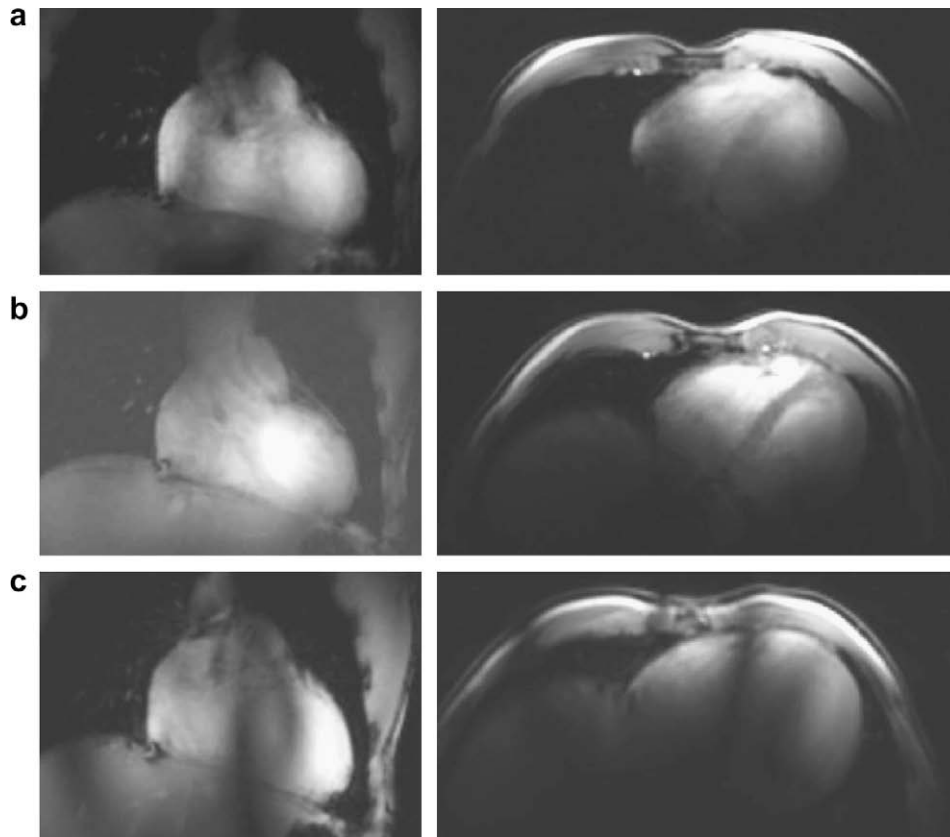
Fig. 2. Coronal (left) and axial (right) low-resolution scout images acquired using different coil configurations. (a) Single loop coil, (b) loop/butterfly pair in quadrature configuration, (c) loop/butterfly pair in an anti-quadrature configuration. Sequence parameters: turboFLASH sequence, TR/TR 4/1.82 ms, in-plane resolution 2.3 × 4.7 mm, slice thickness 10 mm.
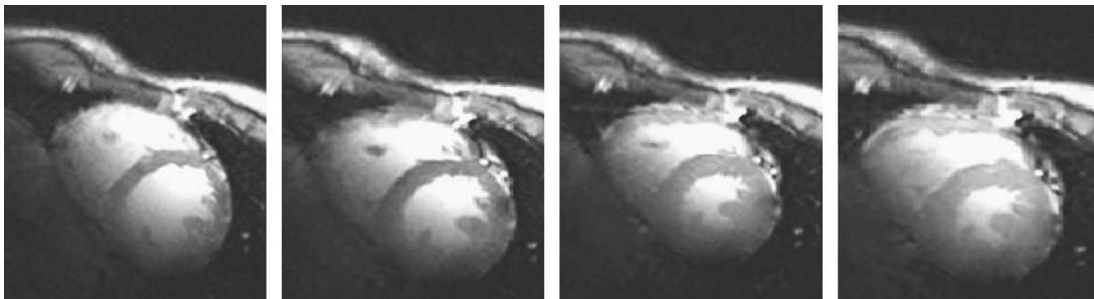

Fig. 3. Images from a short-axis cine sequence. Images are acquired over eight breath-holds with times corresponding to ~25 ms intervals. Shown is every fourth image acquired at times 0, 99, 198 and 297 ms after the R-wave. Data acquisition parameters are listed in the main text.
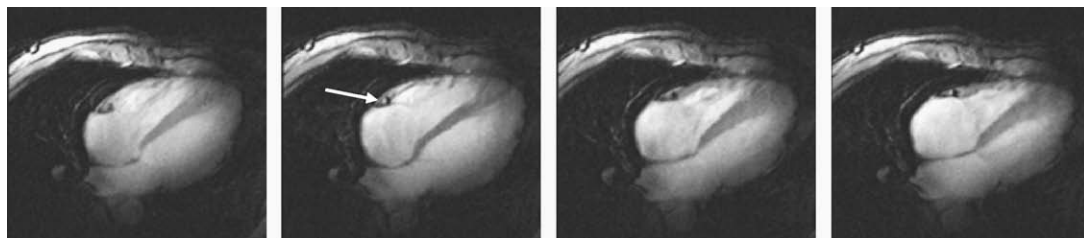

Fig. 4. Images from a four-chamber cine sequence. Images are acquired over eight breath-holds with times corresponding to 27 ms intervals. Every fourth images is shown above at times 108, 216, 324 and 432 ms after the R-wave. Data acquisition parameters are described in the main text. The right coronary artery can also be seen (small arrow) perpendicular to the slice dimension.

which they studied. Our initial step was to estimate the B_1^+ using the same power level as for all the cine sequences. Using the technique outlined previously our estimated B_1^+ at the center of the heart was 1.4 μT (using a 0.6 ms duration half sinc-gauss excitation pulse) and at the surface of the chest was 4.9 μT, c. The results from the Collins and Smith paper were interpolated to values at
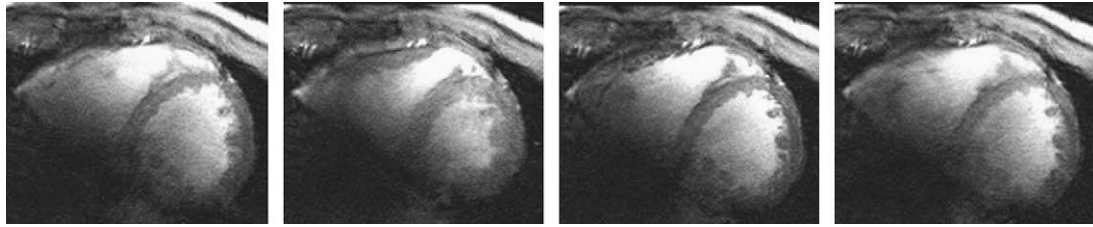
Fig. 5. Every fourth frame from a high-resolution cine sequence showing excellent delineation of the papillary muscles in the myocardium. Images were acquired every ~35 ms.
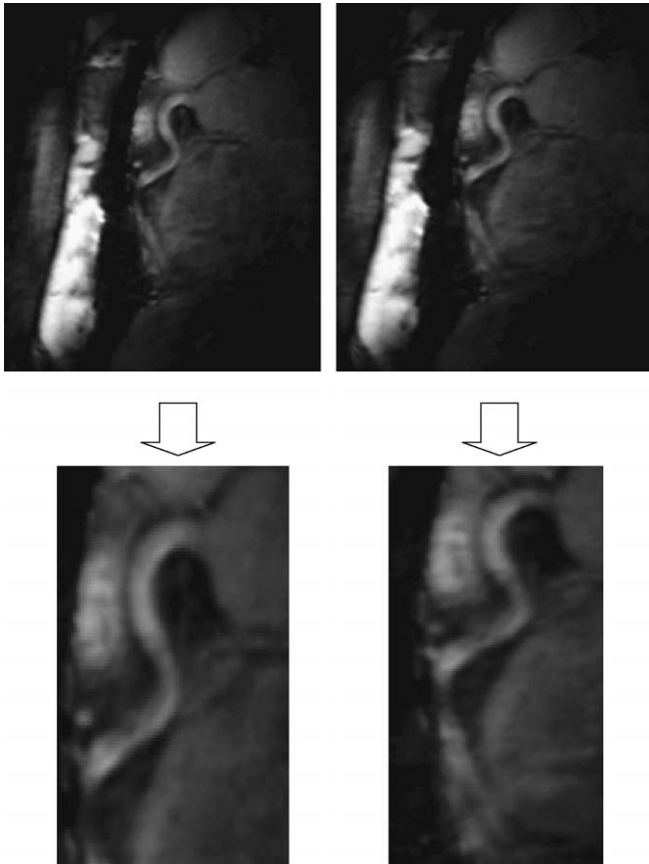
Fig. 6. Two successive slices through a volunteer showing the right coronary artery (top). Expansion of the images showing more clearly the delineation of the artery (bottom).

298.1 MHz since frequencies of 64, 125, 175, 260 and 345 MHz were used in the original simulations. Using the fact that the SAR is proportional to the time integral of the magnitude of the square of the B_1^+ field, we can arrive at approximate SAR values. The SAR in the heart is, as derived from the relative B_1^+ values, negligible compared to that at the chest surface. As noted by Collins and Smith, the local SAR is the limiting factor, since the average SAR is up to two orders of magnitude less. The estimated value of local SAR at the chest surface is ~0.2 W/kg per 1 g of tissue, which is more than a factor-of-four below those of the Food and Drug Administration (FDA) and International Electrotechnical Commission (IEC).

4. Conclusions

Although the optimum RF engineering configuration for high field body imaging will ultimately consist of separate multi-chan-nel transmit and receive arrays, this setup is not widely available at the current time, and there is a sentiment that it is not possible to perform useful body imaging at 7 tesla and above without such technology. The results shown here illustrate that a well-designed simple coil setup is capable of obtaining both cine-cardiac sequences for functional applications, as well as structural information related to, for example, dimensions of the coronary artery.

A number of challenges remain to be addressed. For example, the use of high efficiency balanced imaging sequences is routine at 1.5 tesla, but has proved challenging to implement at 3 tesla [12] and is likely to require sophisticated higher order shimming to be even feasible at 7 tesla. The lack of a body-coil for uniform excitation also makes many standard preparation modules for imaging sequences difficult: for example, black-blood imaging or quantitative velocity measurements. One of the most promising applications for very high field cardiac MR is localized cardiac spectroscopy (both homonuclear and heteronuclear), which has the advantage of significantly enhanced spectral resolution, but again has a number of significant challenges in order to obtain high quality spectra. The aim of this current paper is to show that, even with relatively simple RF coil design, both functional and structural information can be obtained, and that many groups can now apply their expertise acquired at lower fields to the challenges of cardiac MR at 7 tesla and above.

References

[1] G. Adriany, P.F. van de Moortele, J. Ritter, S. Moeller, E.J. Auerbach, C. Akgun, C.J. Snyder, T. Vaughan, K. Ugurbil, A geometrically adjustable 16-channel transmit/receive transmission line array for improved RF efficiency and parallel imaging performance at 7 tesla, Magn. Reson. Med. 59 (2008) 590–597.
[2] J.H. Duyn, G.P. van, T.Q. Li, J.A. de Zwart, A.P. Koretsky, M. Fukunaga, High-field MRI of brain cortical substructure based on signal phase, Proc. Natl. Acad. Sci. U. S. A. 104 (2007) 11796–11801.
[3] A.C. Zelinski, L.L. Wald, K. Setsompop, V. Alagappan, B.A. Gagoski, V.K. Goyal, E. Adalsteinsson, Fast slice-selective radio-frequency excitation pulses for mitigating B_1^+ inhomogeneity in the human brain at 7 tesla, Magn. Reson. Med. 59 (2008) 1355–1364.
[4] R. Krug, J. Carballido-Gamio, S. Banerjee, R. Stahl, L. Carvajal, D. Xu, D. Vigneron, D.A. Kelley, T.M. Link, S. Majumdar, In vivo bone and cartilage MRI using fully-balanced steady-state free-precession at 7 tesla, Magn. Reson. Med. 58 (2007) 1294–1298.
[5] R. Krug, J. Carballido-Gamio, S. Banerjee, A.J. Burghardt, T.M. Link, S. Majumdar, In vivo ultra-high-field magnetic resonance imaging of trabecular bone microarchitecture at 7 T, J. Magn. Reson. Imaging 27 (2008) 854–859.
[6] J. Zuo, R. Bolbos, K. Hammond, X.J. Li, S. Majumdar, Reproducibility of the quantitative assessment of cartilage morphology and trabecular bone structure with magnetic resonance imaging at 7 T, J. Magn. Reson. Imaging 26 (2008) 560–566.
[7] D. Sullivan, Mathematical-methods for treatment planning in deep regional hyperthermia, IEEE Trans. Microwave Theory Tech. 39 (1991) 864–872.

[8] P. Wust, J. Nadobny, R. Felix, P. Deuflhard, A. Louis, W. John, Strategies for optimized application of annular-phased-array systems in clinical hyperthermia, Int. J. Hypertherm. 7 (1991) 157–173.

[9] G.J. Metzger, C. Snyder, C. Akgun, T. Vaughan, K. Ugurbil, P.F. van de Moortele, Local B_1^+ shimming for prostate imaging with transceiver arrays at 7 T based on subject-dependent transmit phase measurements, Magn. Reson. Med. 59 (2008) 396–409.

[10] J.T. Vaughan, C.J. Snyder, L.J. DelaBarre, P.J. Bolan, J. Tian, L. Bolinger, G. Adriany, P. Andersen, J. Strupp, K. Ugurbil, Whole-body imaging at 7 T: preliminary results, Magn. Reson. Med. 61 (2009) 244–248.

[11] C.J. Snyder, L. Delabarre, G.J. Metzger, P.F. van de Moortele, C. Akgun, K. Ugurbil, J.T. Vaughan, Initial results of cardiac imaging at 7 tesla, Magn. Reson. Med. 61 (2009) 517–524.

[12] A.M. Gharib, A. Elagha, R.I. Pettigrew, Cardiac magnetic resonance at high field: promises and problems, Curr. Probl. Diagn. Radiol. 37 (2008) 49–56.

[13] D.I. Hoult, D. Phil, Sensitivity and power deposition in a high-field imaging experiment, J. Magn. Reson. Imaging 12 (2000) 46–67.

[14] E.B. Boskamp, Magnetic Resonance Imaging Apparatus Comprising a Quadrature Coil System, US Patent #4816765, 1989.

[15] J.S. Hyde, A. Jesmanowicz, T.M. Grist, W. Froncisz, J.B. Kneeland, Quadrature detection surface coil, Magn. Reson. Med. 4 (1987) 179–184.

[16] A. Kumar, P.A. Bottomley, Optimized quadrature surface coil designs, MAGMA 21 (2008) 41–52.

[17] B.H. Suits, A.N. Garroway, J.B. Miller, Surface and gradiometer coils near a conducting body: the lift-off effect, J. Magn. Reson. 135 (1998) 373–379.

[18] S. van Elderen, A.G. Webb, M. Versluis, J. Westenberg, J. Doornbos, N.B. Smith, A. de Roos, M. Stuber, *In vivo* human coronary magnetic resonance angiography at 7 Tesla, J. Cardio. Magn. Reson. 11 (2009) O46.

[19] V.L. Yarnykh, Actual flip-angle imaging in the pulsed steady state: a method for rapid three-dimensional mapping of the transmitted radiofrequency field, Magn. Reson. Med. 57 (2007) 192–200.

[20] X. Wu, D.K. Deelchand, V.L. Yarnykh, K. Ugurbil, P.F. van de Moortele, Actual flip angle imaging: from 3D to 2D, Int. Soc. Magn. Reson. Med. 341 (2009) (Abstract).

[21] J. Wang, Q.X. Yang, X. Zhang, C.M. Collins, M.B. Smith, X. Zhu, K. Ugurbil, W. Chen, Polarization of the RF field in a human head at high field: a study with a quadrature surface coil at 7.0 T, Magn. Reson. Med. 48 (2002) 362–369.

[22] C.M. Collins, M.B. Smith, Calculations of B_1 distribution, SNR, and SAR for a surface coil adjacent to an anatomically-accurate human body model, Magn. Reson. Med. 45 (2001) 692–699.